Electronic Supporting Information

Condensed and gaseous benzonitrile: ionic species formation and structures parameters

Jorge Basilio,[a] Ricardo R. Oliveira,*[b] Roberto Nascimento,[a] Maria Luiza M. Rocco,[b] Lucia H. Coutinho,[a] Fabio de A. Ribeiro[c] and Wania Wolff.*[a]

[a] *Physics Institute, Federal University of Rio de Janeiro, Rio de Janeiro, Brazil.*
* *e-mail: rrodrigues.iq@gmail.com*
[b] *Chemistry Institute, Federal University of Rio de Janeiro, Rio de Janeiro, Brazil.*
* *e-mail: wolff@if.ufrj.br*
[c] *Federal Institute of Rio de Janeiro, Nilópolis, RJ 26530-060, Brazil.*

Contents

S1 Cations at Titan and dications in solar atmospheres **S2**

S2 Five, six and larger aromatic cyano rings **S2**

S3 Admission spectrum **S2**

S4 Absolute cross sections **S3**

S5 Vibrational frequencies for isomers **S6**

S6 Geometric parameters **S12**

S7 Energy parameters **S18**

S8 CASSCF Active Space for m/z 105 G.M candidates **S19**

S9 Electron fluxes on Titan ionosphere at different altitudes **S22**

S10 Destruction rate for T40 flyby **S23**

S11 Mean half-life of gaseous $CN-Bz$ under electron impact **S24**

S12 Chemical and dynamical lifetimes **S24**

S13 Cross-Sections as function of the energy-gas phase **S25**

S1 Cations at Titan and dications in solar atmospheres

In Titan several ionic hydrocarbons and cyanides have been detected and some of them are listed in Table S1. Planetary ionospheres contain not only singly-ionized ions, but also doubly charged positive ions[1]. Atomic and diatomic dications have been detected in the atmospheres of Earth[2,3], Venus[4,5], Mars[6–8], Jupiter[9], Io[9–11] and moons of Saturn[12,13]; some of them are listed in Table S1

Table S1 Detected cations at Titan and dications in solar atmospheres

hydrocarbons	**cyanides**		**atomic X^{2+}**	**diatomic XY^{2+}**
C_2H_2	HCN		C^{2+}	
C_2H_4	HNC		O^{2+}	
C_2H_6	HC_3N		N^{2+}	
c-C_3H_2	C_2N_2		S^{2+}	
CH_2CCH_2	CH_3CN			CO^{2+}
CH_3CCH	C_2H_3CN			CO_2^{2+}
C_3H_6	C_2H_5CN			O^{2+}
C_3H_8	CH_3C_3N			N_2^{2+} (Titan)
C_4H_2				NO^{2+} (Titan)
c-C_6H_6				N_2O^{2+} (Titan)

S2 Five, six and larger aromatic cyano rings

The astronomical relevance of $CN-Bz$ was highlighted when several five-membered rings (1-cyano-1,3-cyclopentadiene (1-cyano-CPD, $c-C_5H_5CN$) and six-membered aromatic rings, such as $CN-Bz$ itself, were detected within the interstellar Taurus molecular cloud (TMC-1) using radio astronomy[14–19]. Its possible presence in protostellar sources such as Serpens 1A, Serpens 1B, Serpens 2 and MC27/L1521F[18] is strongly considered. Large aromatic cyano molecules were detected in TMC-1, cyanoacenaphthylene[20] and cyanopyrene[21]

S3 Admission spectrum

During admission/injection of gaseous benzonitrile molecules, the pressures of selected ion masses were measured by a residual gas analyzer (quadrupole mass spectrometer RGA-200) and recorded as functions of injection time.

The measurement allows monitoring and control of the admission by identifying the amounts of gases present in the chamber during the deposition procedure. The thickness of the film can also be estimated.

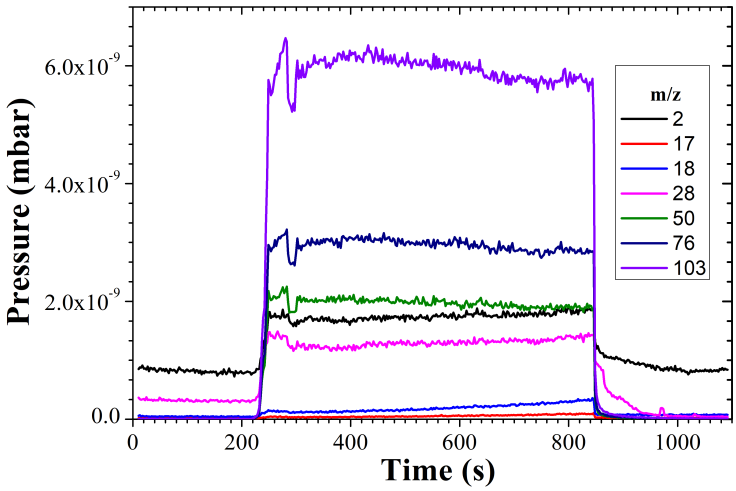

Figure S1 Pressure of selected masses as function of the injection time measured by a quadrupole mass spectrometer

S4 Absolute cross sections

The absolute total cross sections (TICS) and partial cross sections (PICS) are listed in Table S2 for four selected electron impact energies: 16, 70, 600 and 2000 eV. They are given in $1 \cdot 10^{-16}$ cm^2. All detected mass/charge species are listed. At the lowest measured electron energy of 12 eV only the parent ion was accessible. The assignment to molecular species is indicated in Figure 2 (main text).

Figure S2 presents a representative view of the non-dissociative and dissociative ionization cross sections (PICS) normalized to the absolute total ionization cross sections (TICS) of $CN-Bz$[22] for sixteen electron impact energies.

Table S2 Absolute total and partial cross sections for the electron impact energies of 16, 70, 600 and 2000 eV given in $1 \cdot 10^{-16}$ cm^2.

Energy	16	70	600	2000
Qion	2,646	15,997	6,566	2,622
103	–	8,627	3,826	1,543
104	–	0,803	0,329	0,144
105	–	0,0582	0,0285	0,0122
parent ion	2,536	9,488	4,183	1,703
all frag ion	0,110	6,509	2,383	0,920
102	–	0,0866	0,0385	0,0136
101	–	0,013	0,0044	0,0017
100	–	0,0294	0,0071	0,0016
99	–	0,0551	0,0141	0,0035
98	–	0,0082	0,0013	2,9E-04
89	–	0,0069	0,0043	0,0018
88	–	0,0275	0,0106	0,0036
87	–	0,0097	0,0029	7,7E-04
86	–	0,0117	0,0021	4,3E-04
85	–	0,0076	0,0023	7,4E-04
84	–	0,0208	0,0079	0,0025
78	–	0,143	0,0382	0,0144
77	0,037	0,380	0,190	0,0569
76	0,07	1,548	0,886	0,396
75	–	0,425	0,102	0,0391
74	–	0,173	0,0322	0,0105
73	–	0,0536	0,00934	0,00184
72	–	0,0083	0,0019	5,6E-04
65	–	0,0251	0,0128	0,0067
64	–	0,0766	0,0279	0,01
63	0,0025	0,134	0,0511	0,0190
62	–	0,0508	0,0115	0,0042
61	–	0,0420	0,0077	0,0017
60	–	0,0111	0,0017	2,5E-04
53	–	0,0605	0,0205	0,0079
52	–	0,321	0,121	0,0516
51,5	–	0,335	0,0984	0,0320
51	–	0,477	0,145	0,0553
50,5	–	0,129	0,0336	0,0112
50	–	0,850	0,267	0,0978
49	–	0,117	0,0190	0,0041
48	–	0,0153	0,0027	3,5E-04
40	–	0,0241	0,0091	0,0030
39	–	0,332	0,0925	0,0364
38	–	0,194	0,0336	0,0101
37	–	0,158	0,0275	0,0079
36	–	0,0175	0,0049	5,4E-04
27	–	0,100	0,0269	0,0076
26	–	0,12902	0,02838	0,00996
25	–	0,0073	0,0017	1,5E-04
1	–	0,0240	0,0166	0,0032
15	–	6,0E-04	4,2E-04	1,4E-04
14	–	0,0033	0,0043	9,5E-04
13	–	3,5E-05	4,2E-05	0
12	–	3,8E-04	5,1E-04	1,0E-04

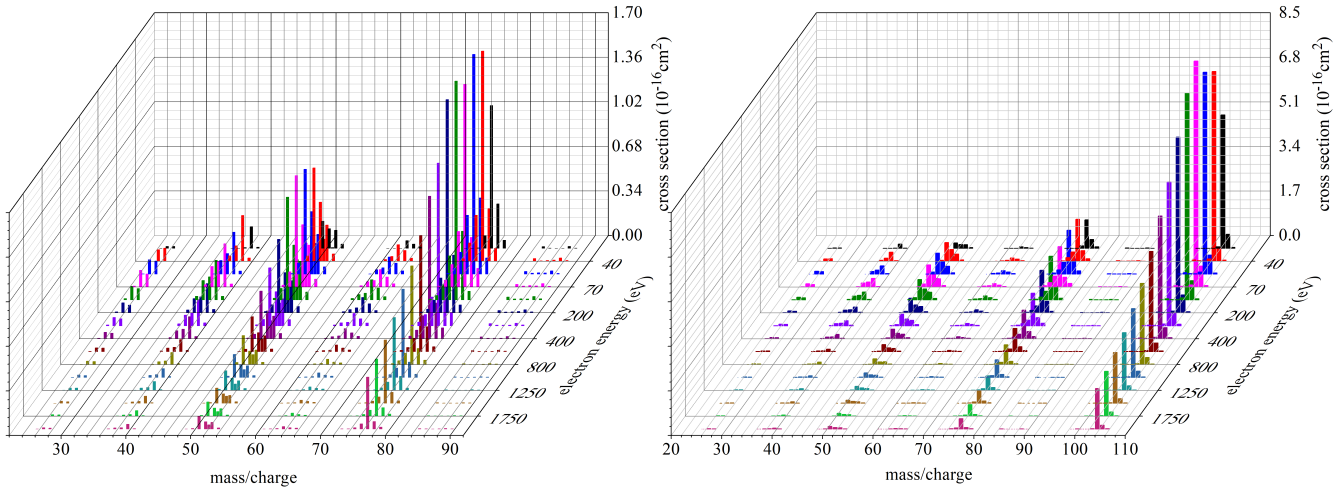

Figure S2 Absolute cross sections of $CN-Bz$ at sixteen electron energies starting at 20 eV and ending at 2000 eV in the units of 10^{-16} cm^2. The color variation highlights the cross sections at representative electron impact energies. Present measured relative cross sections were normalized with respect to BEBωB97-X total ionization cross section of reference[22]. Right panel: Cross sections of all ionic species of groups $A-G$ (see Figure 2 main text) as a function of the m/z ratio; Left panel: only for the fragment ions.

S5 Vibrational frequencies for isomers

The vibrational frequencies of each isomer candidate for the global minimum are shown in Tables S3, S4, S5, S6 and S7 ensuring that they are local minima. Each table contains the set of isomers corresponding to each m/z. For convenience, the normal modes of vibration that are null have been omitted.

Table S3 Vibrational frequencies (cm^{-1}) for the isomers 6.1^+, 6.2^+, 6.3^+, 6.4^+ e 6.5^+.

mode	**frequencies (cm^{-1})**				
	6.1^+	**6.2^+**	**6.3^+**	**6.4^+**	**6.5^+**
6	132	136	139	157	244
7	155	153	154	294	281
8	295	340	343	450	347
9	389	393	398	480	434
10	390	489	482	545	549
11	461	527	522	640	586
12	584	536	551	669	669
13	585	640	637	685	753
14	606	745	684	726	777
15	639	753	743	795	804
16	686	762	748	856	833
17	780	782	798	887	836
18	781	798	803	894	908
19	854	844	864	932	938
20	973	934	952	953	967
21	1003	1010	993	973	990
22	1016	1031	1041	980	1001
23	1046	1055	1048	1034	1079
24	1051	1074	1076	1066	1087
25	1124	1126	1136	1133	1133
26	1200	1196	1213	1189	1186
27	1204	1268	1260	1214	1221
28	1249	1281	1306	1284	1274
29	1346	1350	1365	1321	1349
30	1387	1408	1377	1426	1453
31	1486	1494	1501	1469	1520
32	1518	1578	1594	1533	1558
33	1623	1659	1653	1593	1579
34	1648	1683	1685	1661	1676
35	2350	2244	2245	1677	1749
36	3210	3219	3224	3242	3229
37	3218	3239	3239	3249	3238
38	3221	3245	3248	3258	3255
39	3231	3250	3252	3273	3264
40	3234	3446	3454	3278	3284
41	3741	3570	3574	3622	3573

Table S4 Vibrational frequencies (cm^{-1}) for the isomers 7.1^+, 7.2^+, 7.3^+, 7.4^+ e 7.5^+.

mode	**frequencies (cm^{-1})**				
	7.1^+	**7.2^+**	**7.3^+**	**7.4^+**	**7.5^+**
6	187	199	199	205	120
7	250	241	265	292	151
8	401	387	382	335	274
9	448	455	449	452	378
10	541	556	561	594	456
11	646	654	636	685	458
12	693	663	638	688	479
13	726	682	702	692	539
14	737	707	711	698	651
15	800	737	734	749	708
16	863	802	831	774	715
17	874	857	861	822	786
18	911	903	870	866	847
19	953	918	898	870	857
20	961	945	924	919	906
21	972	950	953	934	924
22	994	985	985	946	993
23	1037	1039	1033	981	993
24	1086	1059	1090	1109	1014
25	1101	1095	1129	1113	1063
26	1180	1149	1152	1121	1121
27	1197	1165	1186	1172	1195
28	1245	1250	1222	1210	1238
29	1262	1299	1296	1284	1275
30	1314	1338	1307	1290	1317
31	1340	1380	1363	1309	1395
32	1423	1398	1405	1346	1418
33	1429	1418	1444	1386	1493
34	1468	1474	1491	1467	1509
35	1501	1518	1497	1490	1626
36	1557	1535	1592	1580	1695
37	1573	1628	1662	1623	1963
38	3061	3057	3051	3026	3104
39	3103	3091	3081	3048	3178
40	3249	3237	3233	3248	3238
41	3261	3254	3254	3253	3238
42	3269	3271	3274	3282	3250
43	3272	3290	3281	3287	3251
44	3285	3631	3628	3600	3605

Table S5 Vibracional frequencies (cm^{-1}) for the isomers 8.1^+, 8.2^+, 8.3^+, 8.4^+ e 8.5^+.

mode	**frequencies (cm^{-1})**				
	8.1^+	**8.2^+**	**8.3^+**	**8.4^+**	**8.5^+**
6	96	50	196	177	121
7	221	193	213	231	236
8	225	238	407	389	294
9	397	411	417	420	449
10	428	439	474	481	559
11	450	450	562	556	659
12	583	559	663	646	668
13	621	630	713	686	734
14	665	654	769	732	775
15	695	749	814	783	815
16	741	781	824	822	834
17	808	813	897	885	903
18	814	870	918	891	907
19	845	907	968	942	938
20	965	1001	995	942	960
21	998	1007	1051	1006	983
22	1017	1017	1052	1041	1027
23	1044	1028	1067	1055	1049
24	1052	1032	1133	1108	1049
25	1070	1048	1153	1149	1103
26	1112	1084	1183	1180	1160
27	1149	1137	1194	1190	1201
28	1199	1228	1196	1225	1231
29	1213	1262	1226	1239	1244
30	1273	1292	1249	1251	1292
31	1366	1329	1301	1297	1324
32	1406	1363	1321	1325	1337
33	1409	1425	1390	1425	1373
34	1494	1462	1454	1437	1436
35	1534	1543	1478	1464	1447
36	1601	1557	1506	1508	1487
37	1632	1652	1536	1582	1505
38	1660	1684	1650	1668	1632
39	1729	1708	1687	1695	1707
40	3193	3176	3111	3092	3060
41	3193	3190	3115	3101	3090
42	3201	3229	3165	3143	3099
43	3211	3238	3185	3158	3149
44	3226	3247	3216	3231	3243
45	3231	3250	3235	3239	3254
46	3563	3267	3241	3243	3269
47	3673	3594	3246	3588	3283

Table S6 Vibrational frequencies (cm^{-1}) for the isomers 3.1^{2+}, 3.2^{2+}, 3.3^{2+}, 3.4^{2+} e 3.5^{2+}.

mode	**frequencies (cm^{-1})**				
	3.1^{2+}	**3.2^{2+}**	**3.3^{2+}**	**3.4^{2+}**	**3.5^{2+}**
6	61	61	61	61	61
7	63	63	63	63	63
8	151	151	151	151	151
9	154	154	154	154	154
10	271	271	271	271	271
11	290	290	290	290	290
12	402	402	402	402	402
13	471	471	471	471	471
14	481	481	481	481	481
15	516	516	516	516	516
16	527	527	527	527	527
17	537	537	537	537	537
18	544	544	544	544	544
19	596	596	596	596	596
20	655	655	655	655	655
21	842	842	842	842	842
22	917	917	917	917	917
23	938	938	938	938	938
24	1260	1260	1260	1260	1260
25	1367	1367	1367	1367	1367
26	1866	1866	1866	1866	1866
27	2090	2090	2090	2090	2090
28	2225	2225	2225	2225	2225
29	2393	2393	2393	2393	2393
30	3032	3032	3032	3032	3032
31	3107	3107	3107	3107	3107
32	3592	3592	3592	3592	3592

Table S7 Vibrational frequencies (cm^{-1}) for the isomers 5.1^{2+}, 5.2^{2+}, 5.3^{2+}, 5.4^{2+} e 5.5^{2+}.

mode	**frequencies (cm^{-1})**				
	5.1^{2+}	**5.2**$^{2+}$	**5.3**$^{2+}$	**5.4**$^{2+}$	**5.5**$^{2+}$
6	158	71	138	62	52
7	166	82	167	74	75
8	401	148	359	142	131
9	414	167	380	181	170
10	421	367	408	340	342
11	488	403	504	357	344
12	515	410	541	403	391
13	533	487	579	460	469
14	585	559	587	554	543
15	589	569	611	563	546
16	645	657	658	571	642
17	706	679	692	590	675
18	741	764	709	762	701
19	789	837	810	810	883
20	935	877	907	810	890
21	936	912	937	938	900
22	950	953	987	973	954
23	1040	989	1007	1024	1002
24	1043	1015	1060	1038	1029
25	1146	1039	1117	1187	1108
26	1178	1130	1164	1232	1233
27	1199	1254	1211	1302	1281
28	1283	1331	1271	1346	1337
29	1385	1404	1379	1375	1372
30	1415	1437	1441	1423	1410
31	1529	1792	1511	1791	1786
32	1808	2028	1799	2302	2348
33	2403	2401	2399	2446	2423
34	3170	3108	3152	3004	3001
35	3172	3129	3178	3034	3037
36	3184	3238	3187	3234	3237
37	3189	3271	3215	3268	3272
38	3593	3623	3585	3629	3615

S6 Geometric parameters

The geometric parameters, such as Loewdin charge distribution, bond angles, and bond lengths of each Global Minima candidate, are shown in FiguresS3,S4,S5,S6,S7,S8,S9,S10 S11and S12. In these figures the atoms are indicated in colors: carbons atoms are gray, hydrogens atoms are white, and nitrogen atoms are blue.

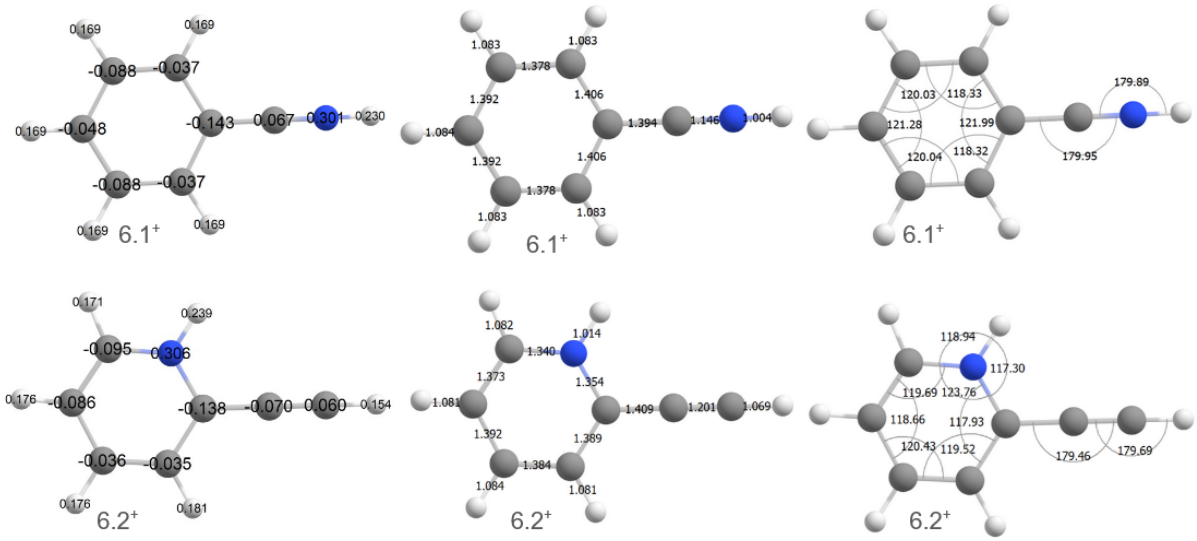

Figure S3 Structural parameters (charge distribution, bond lengths and angles) for 6.1^{+} and 6.2^{+}Global Minimum candidates

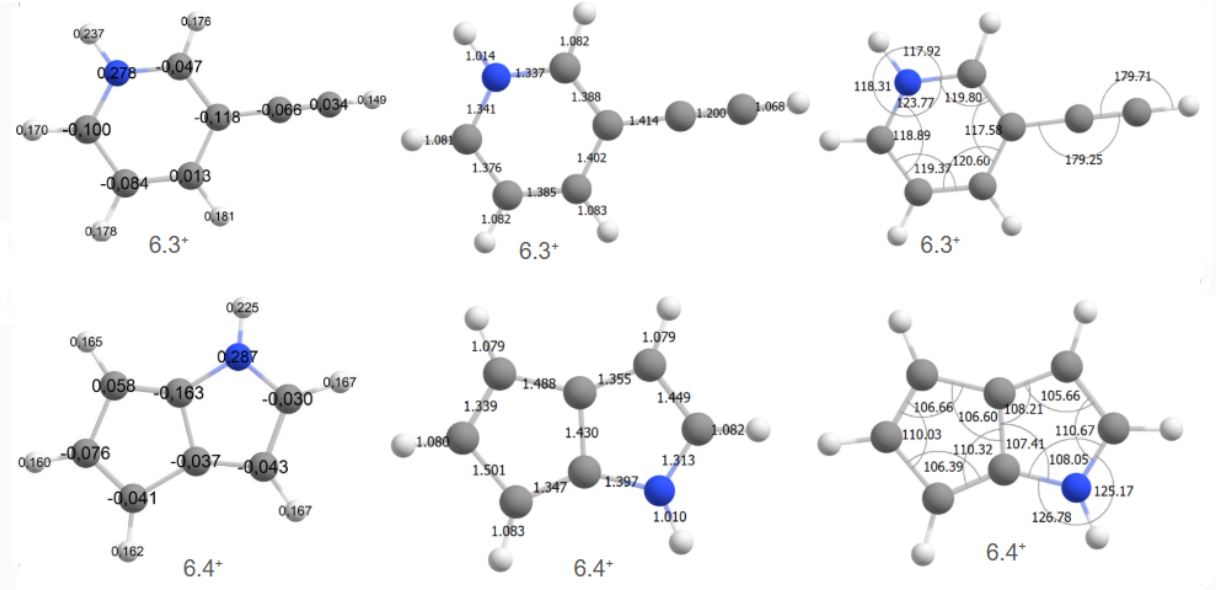

Figure S4 Structural parameters for 6.3^{+} and 6.4^{+} GM candidates

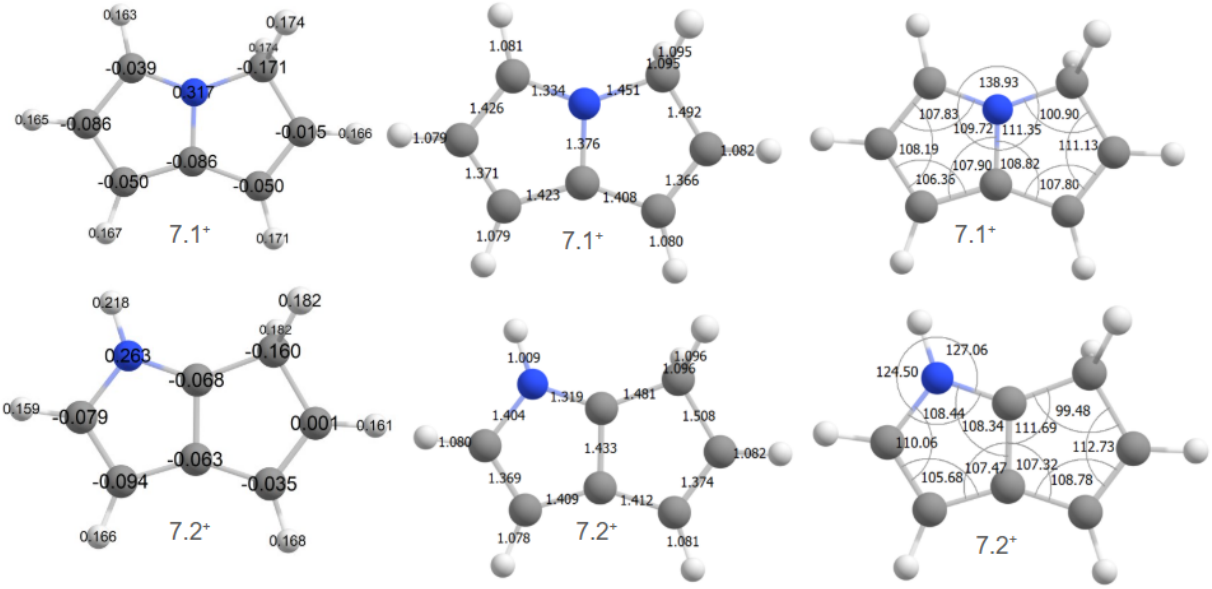

Figure S5 Structural parameters (loewdin charge distribuction, bond lenghts and bond angles) for 7.1^{+} and 7.2^{+}Global Minimum candidates

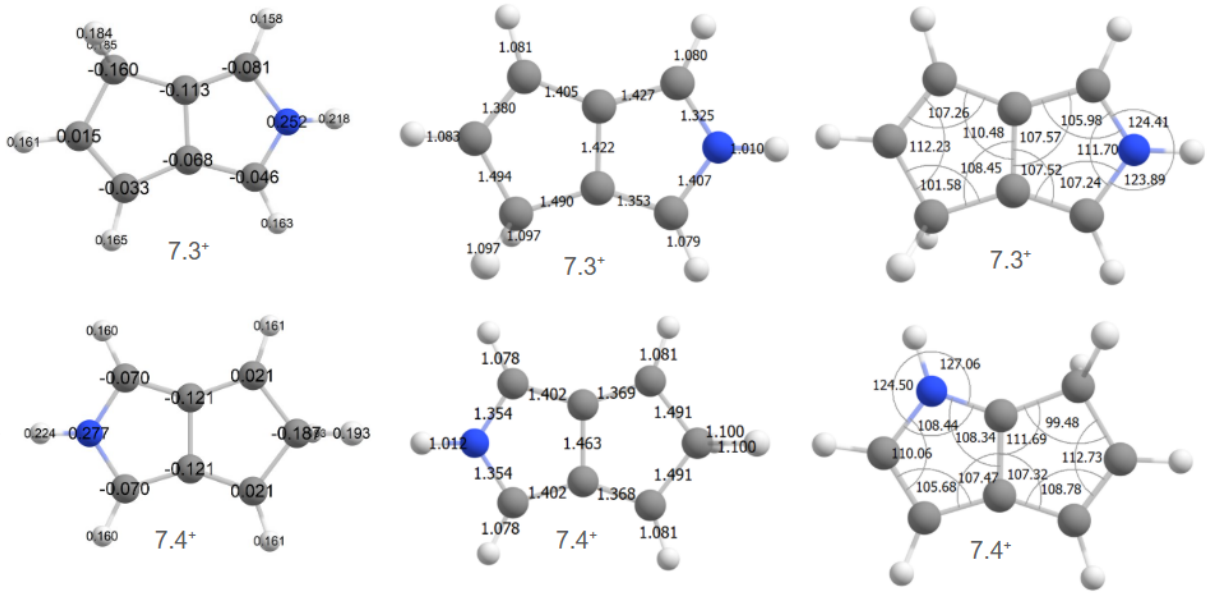

Figure S6 Structural parameters for 7.3^{+} and 7.4^{+} GM candidates

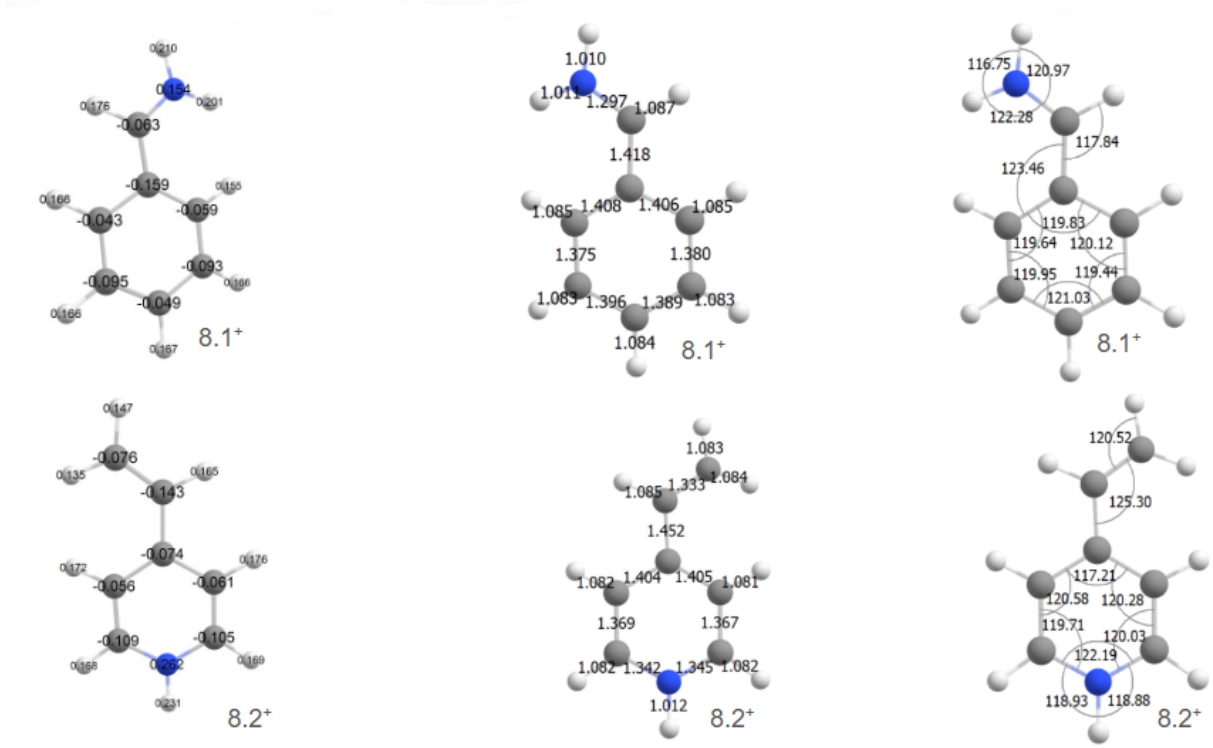

Figure S7 Structural parameters (loewdin charge distribuction, bond lenghts and bond angles) for 8.1^{+} and 8.2^{+}Global Minimum candidates

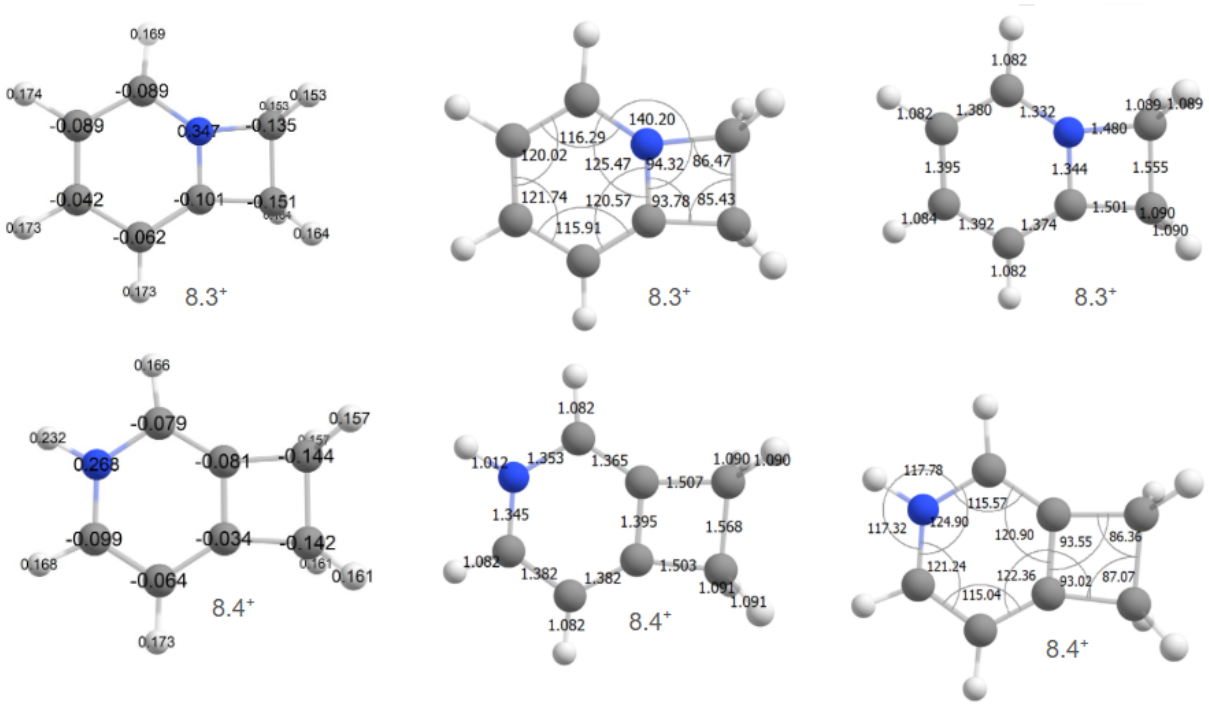

Figure S8 Structural parameters for 8.3^{+} and 8.4^{+} GM candidates

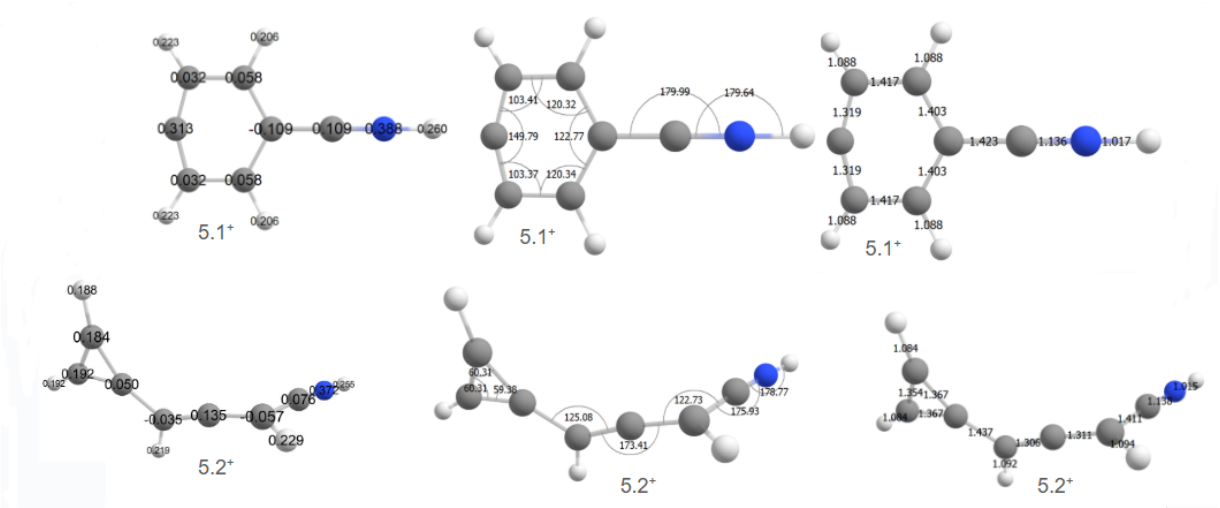

Figure S9 Structural parameters for 5.1^{+} and 5.2^{+} GM candidates

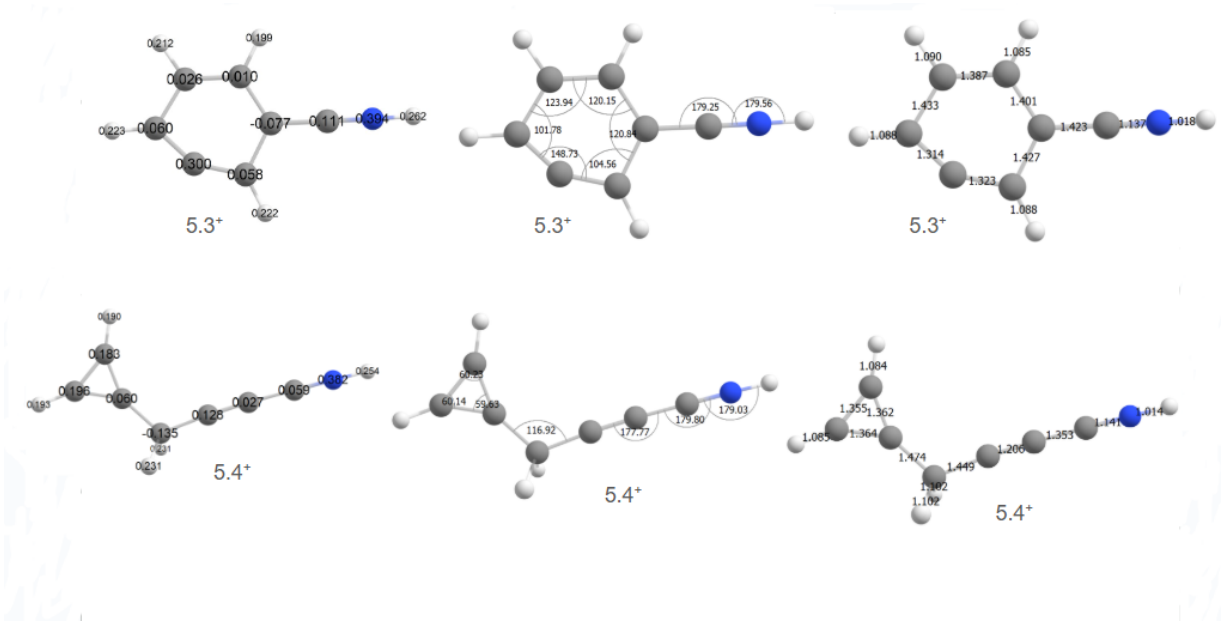

Figure S10 Structural parameters for 5.3^{+} and 5.4^{+} GM candidates

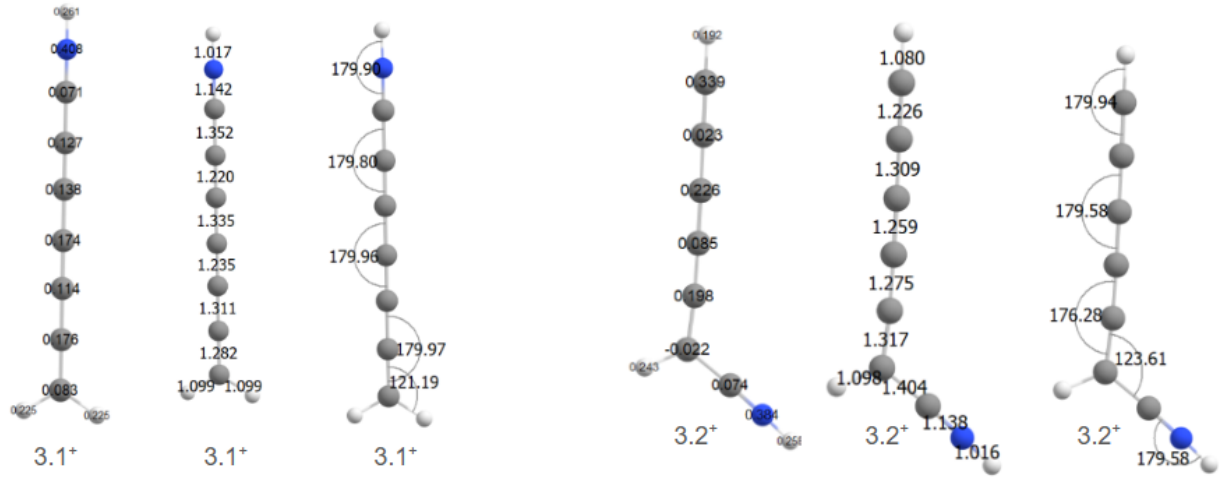

Figure S11 Structural parameters for 3.1^{+} and 3.2^{+} GM candidates

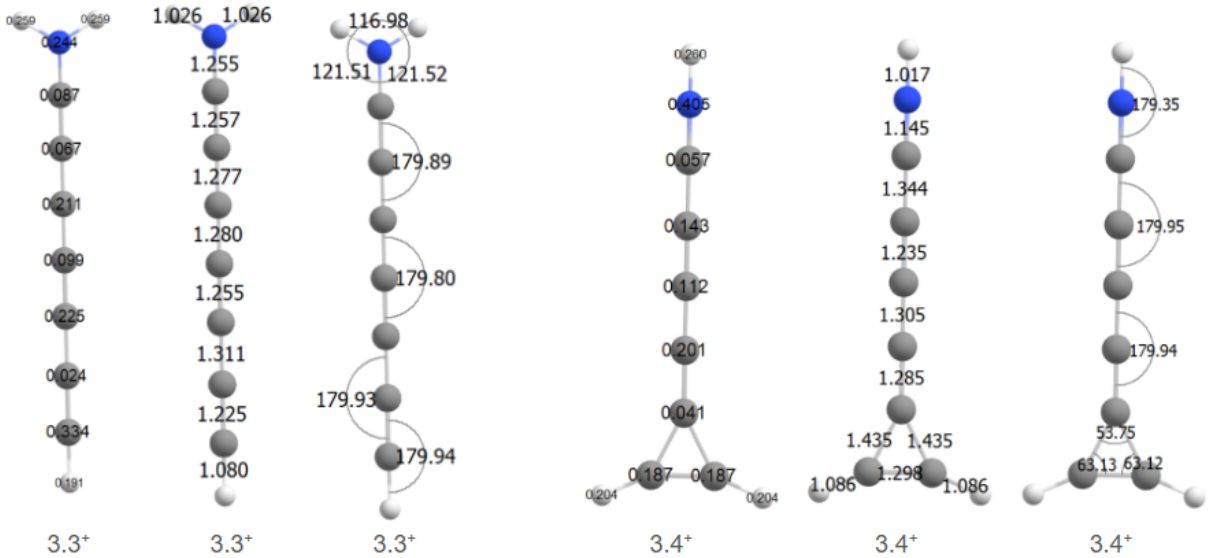

Figure S12 Structural parameters for 3.3^+ and 3.4^+ GM candidates

S7 Energy parameters

The energy differences obtained by DFT (PBE0 / def2-TZVP), CCSD (T) (cc-pVTZ) and it's diagnostics and by CASSCF (NEVPT2 / def2-TZVP) for isomer groups wich at least one candidate has presented T1 $\geq$ 0.03 are shown. The molecules are organized into tables according to their m/z, tablesS8,S9,S10,S11 and S12.

Table S8 Energy parameters for m/z 50.5 GM candidates

Structure	**3.1**$^{2+}$	**3.2**$^{2+}$	**3.3**$^{2+}$	**3.4**$^{2+}$
ΔE (DFT)	0.0	5.70	9.86	11.06
ΔE (CCSD(T))	0.0	2.93	12.80	17.26
T1 diagnostic	0.027	0.021	0.024	0.026

Table S9 Energy parameters for m/z 51.5 GM candidates

Structure	**5.1**$^{2+}$	**5.2**$^{2+}$	**5.3**$^{2+}$	**5.4**$^{2+}$
ΔE (DFT)	0.0	3.54	4.32	8.33
ΔE (CCSD(T))	0.0	4.47	4.44	7.34
T1 diagnostic	0.017	0.013	0.018	0.013

Table S10 Energy parameters m/z 104 GM candidates

Structure	**6.1**$^{+}$	**6.2**$^{+}$	**6.3**$^{+}$	**6.4**$^{+}$
ΔE (DFT)	0.0	12.75	14.43	19.76
ΔE (CCSD(T))	0.0	10.47	11.75	19.53
T1 diagnostic	0.013	0.013	0.013	0.018

Table S11 Energy parameters for m/z 105 GM candidates

Structure	**7.1**$^{+}$	**7.2**$^{+}$	**7.3**$^{+}$	**7.4**$^{+}$
ΔE (DFT)	0.0	0.29	2.02	5.53
ΔE (CCSD(T))	0.0	1.0	3.0	8.6
T1 diagnostic	0.024	0.030	0.029	0.033
ΔE (CASSCF/NEVPT2)	0.0	3.46	4.92	6.5

Table S12 Energy parameters for m/z 106 GM candidates

Structure	**8.1**$^{+}$	**8.2**$^{+}$	**8.3**$^{+}$	**8.4**$^{+}$
ΔE (DFT)	0.0	7.05	11.33	14.65
ΔE (CCSD(T))	0.0	5.62	12.18	16.83
T1 diagnostic	0.013	0.013	0.012	0.012

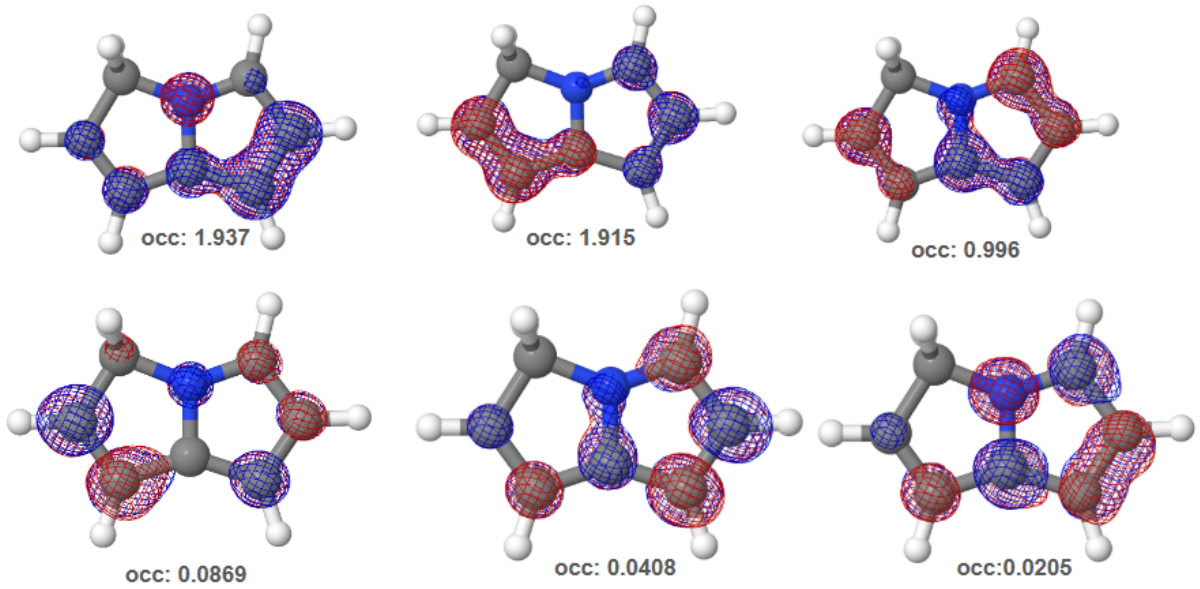

Figure S13 Active space orbitals for 7.1^{+} GM candidates

S8 CASSCF Active Space for m/z 105 G.M candidates

This section shows the active space orbitals of CASSCF, that is, those that had occupancies greater than 0 and less than 2.

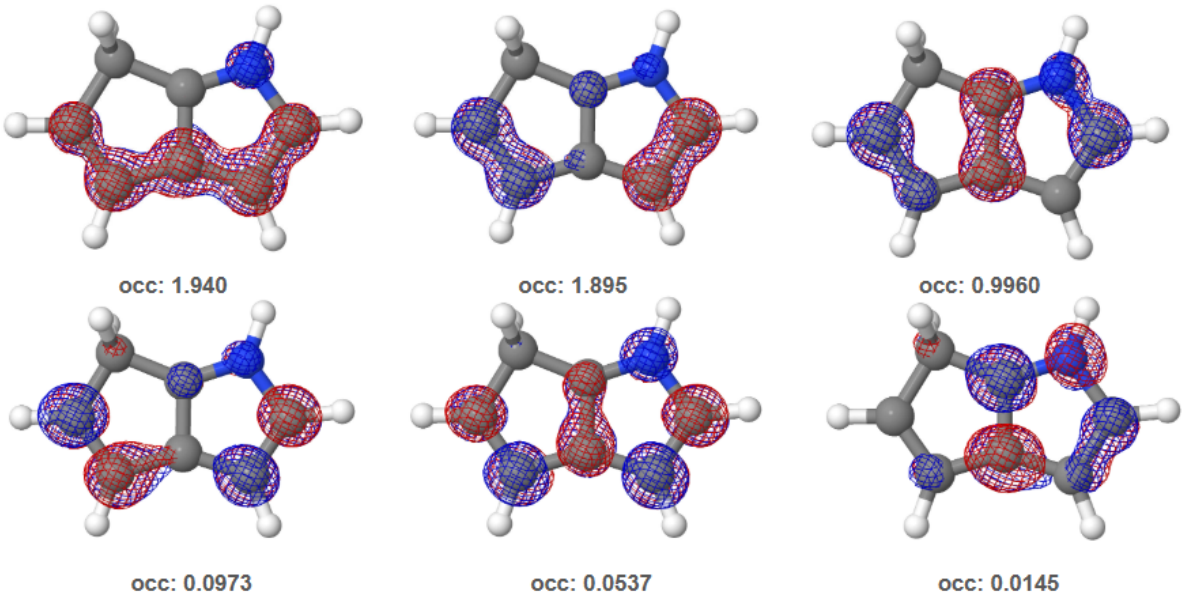

Figure S14 Active space orbitals for 7.2^{+} GM candidates

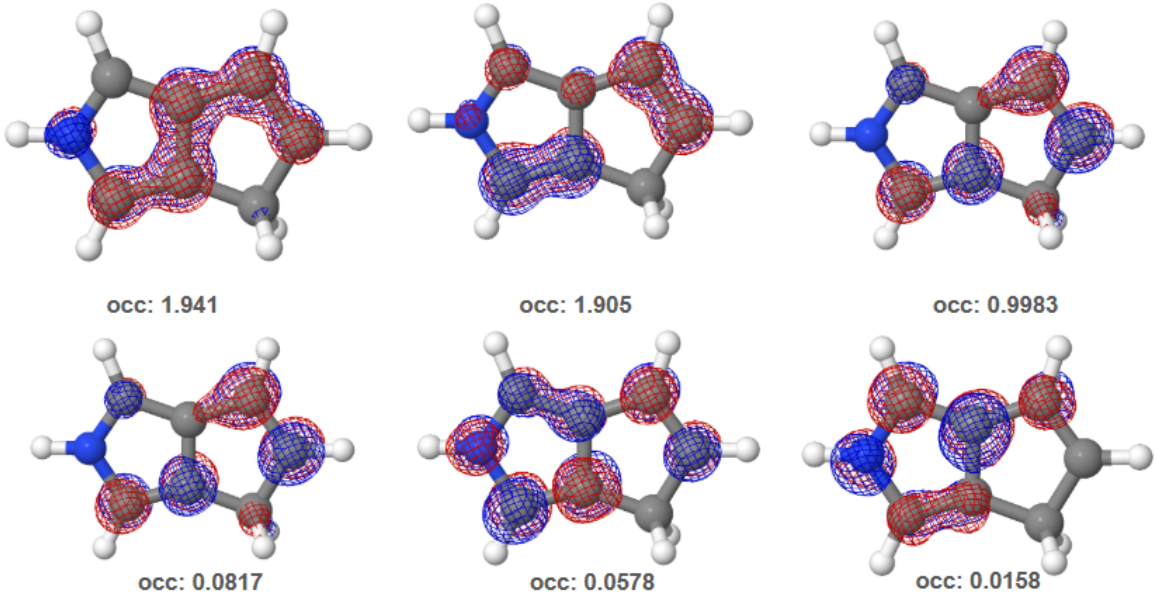

Figure S15 Active space orbitals for 7.3^{+} GM candidates

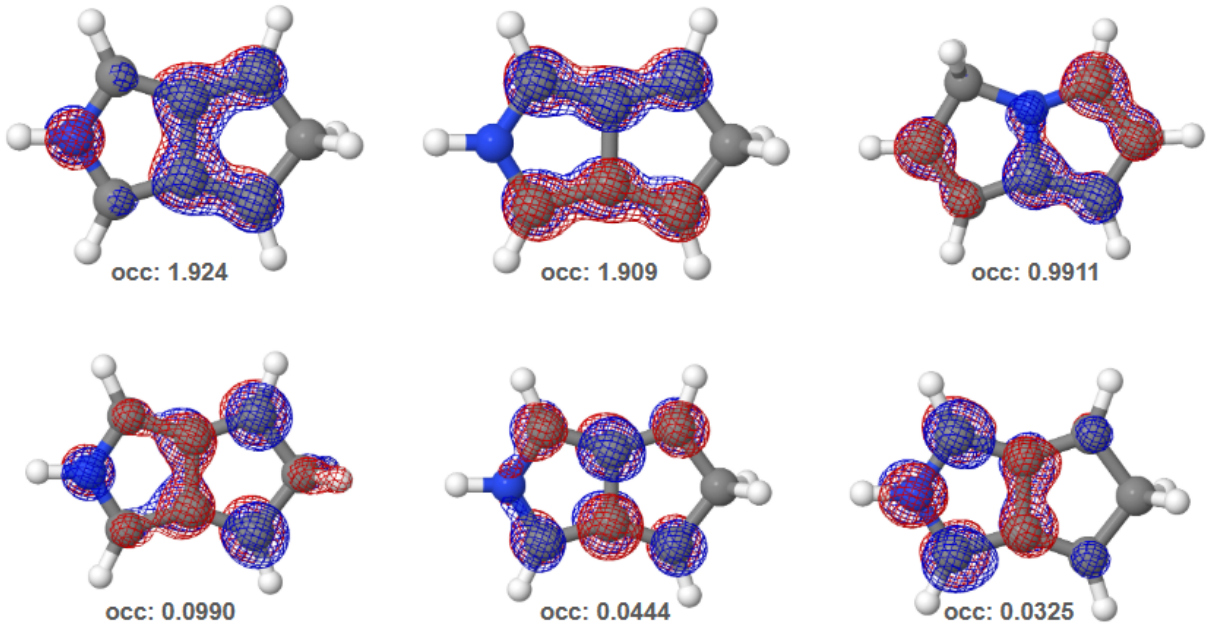

Figure S16 Active space orbitals for 7.4^{+} GM candidates

S9 Electron fluxes on Titan ionosphere at different altitudes

Within the measured electron energy range, we used the data from Plasma-Electron Spectrometers at altitudes ranging from 984 to 2700 km ([23–25]), by Voyager spacecraft from 650 to 1250 km ([26]).

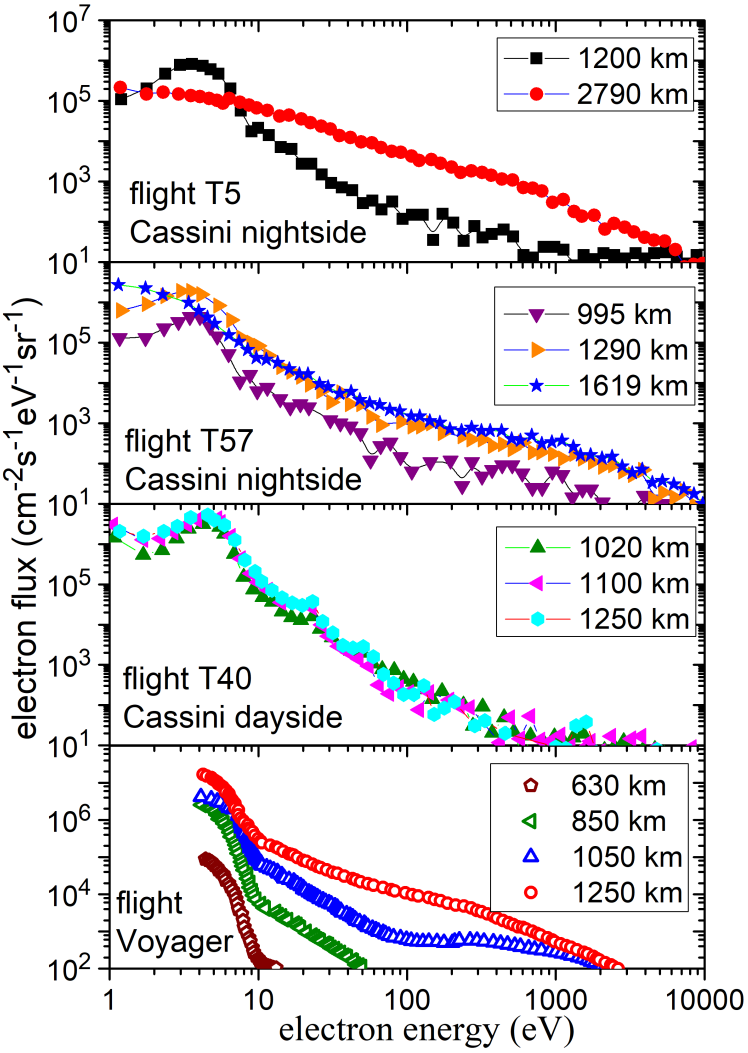

Figure S17 Electron fluxes that impinge on Titan ionosphere at different altitudes

S10 Destruction rate for T40 flyby

The destruction rate as a function of the electron impact energy for the electron flux measured by Cassini for flyby T40 at the night-side face of Titan determined following Equation 2.

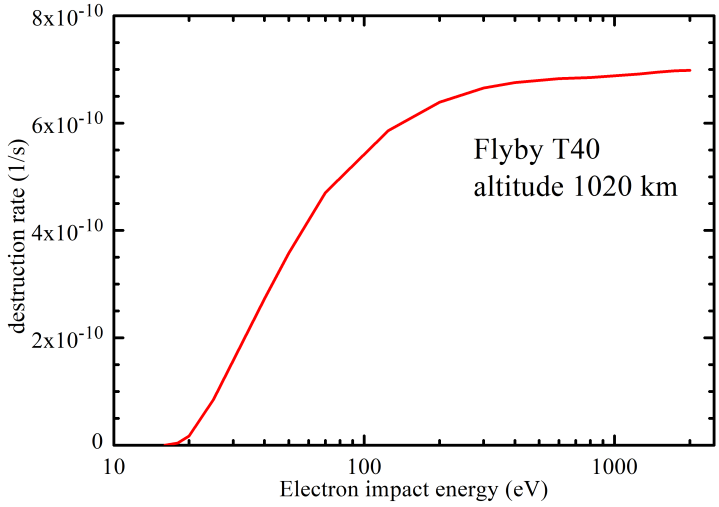

Figure S18 Destruction rate as function of the electron impact energy graphelectronflux.pngfor flyby T40 at 1020 km.

S11 Mean half-life of gaseous $CN-Bz$ under electron impact

The formation rate constant of charged ions, k_f, and the destruction rate, k_d, allow estimation of the half-life of $CN-Bz$[27,28]. The destruction rates are derived from the sum of all fragment partial ionization cross sections multiplied by the integrated electron flux in energy. The following expressions were proposed in references[27–29] and are used to estimate the half-life of molecules under photon impact and other collision processes. It should be noted that chemical and dynamic losses are not included in the evaluation and, therefore, the values reflect an upper limit.

$$k_f = \int_{Emin}^{Emax} \sigma_f(E) flux_{electron}(E) dE \tag{1}$$

$$k_d = \int_{Emin}^{Emax} \sigma_d(E) flux_{electron}(E) dE \tag{2}$$

$$\tau_{1/2} = ln2/k_d \tag{3}$$

where $\sigma_f(E)$ and $\sigma_d(E)$ are the formation cross section of a fragment and the destruction cross section of $CN-Bz$ at an energy E, respectively, $flux_{electron}(E)$ the electron flux at an energy E and $\tau_{1/2}$ is defined as half-life. The cross sections were measured in the impact electron energy range which superimposes the electron energy ranges of the fluxes measured in Titan. The mean half-life of gaseous $CN-Bz$ under electron impact was estimated, which depends on the absolute destruction cross sections and electron fluxes that impinge on Titan ionosphere at different altitudes.

S12 Chemical and dynamical lifetimes

The chemical and dynamical lifetimes, the first related to the total loss rate and the second taking into account the eddy and molecular diffusion of the species at given altitudes, are parameters extracted by nominal models[30,31]. The chemical and dynamical lifetimes of several species, including nitriles, are strongly dependent on altitude, but values were found to differ between works[30–32]. From 200 - 1200 km, the nominal models estimate values ranging from 0.73 years for benzene, 13.2 years for HCN, and 27.7 years for CH_3CN.

S13 Cross-Sections as function of the energy-gas phase

For low-energy regimes, i.e., energies slightly above the ionization energy, the scattering amplitude and, therefore, the cross section are defined by Wannier's law.[33]

$$\sigma \propto E^{1.13} \tag{4}$$

In this low-energy regime, the projectile electron and the one that was stripped from the molecule spend most of their time in the Coulombic region. This power law explains the initial behavior of molecular fragmentation at low energy.[33].

In the energy range between 60 and 150 eV, effects described by the Bethe surface predominate. In this specific region, the energy transfer from the projectile to the molecule is approximately equal to the recoil energy of a free electron ($Q = (\hbar K)^2/(2m)$). In other words, we have the maximum cross-section region.[34].

For high energies, fast electrons collide. In this regime, what matters for cross section is the electric potential of the molecule. We start from the relationship described by Bethe based on Born's first approximation[34,35]. Considering that in a fast process, due to the tendency to have a smooth transfer moment, the form factor will tend to a constant, which will lead to Born's first approximation to an Ln. We will have a ratio for the collision cross section of the type

$$\sigma(E) \propto \frac{\ln(E)}{E} \tag{5}$$

In this region (above 200 eV), the faster the projectile, the smaller the cross section, since $\ln(E) < E$. Thus, the behavior in the gas phase at 2000 eV follow the pattern for high energies, i.e., lower yields than at 1000 eV.The interaction time gets smaller as the electron energy increases.

References

[1] R. Thissen, O. Witasse, O. Dutuit, C. S. Wedlund, G. Gronoff and J. Lilensten, *Physical chemistry chemical physics : PCCP*, 2011, **13 41**, 18264–87.

[2] E. L. Breig, M. R. Torr, D. G. Torr, W. B. Hanson, J. H. Hoffman, J. C. Walker and A. O. C. Nier, *Journal of Geophysical Research*, 1977, **82**, 1008–1012.

[3] C. Simon, J. Lilensten, O. Dutuit, R. Thissen, O. Witasse, C. Alcaraz and H. Soldi-Lose, *Annales Geophysicae*, 2005, **23**, 781–797.

[4] G. Gronoff, J. Lilensten, C. Simon, O. Witasse, R. Thissen, O. Dutuit and C. Alcaraz, *Astronomy and Astrophysics*, 2007, **465**, 641–645.

[5] S. Ghosh, K. K. Mahajan, J. M. Grebowsky and N. Nath, *Journal of Geophysical Research: Space Physics*, 1995, **100**, 23983–23991.

[6] O. Witasse, O. Dutuit, J. Lilensten, R. Thissen, J. Zabka, C. Alcaraz, P.-L. Blelly, S. W. Bougher, S. Engel, L. H. Andersen and K. Seiersen, *Geophysical Research Letters*, 2002, **29**, 104–1–104–4.

[7] O. Witasse, O. Dutuit, J. Lilensten, R. Thissen, J. Zabka, C. Alcaraz, P.-L. Blelly, S. W. Bougher, S. Engel, L. H. Andersen and K. Seiersen, *Geophysical Research Letters*, 2003, **30**,.

[8] E. Dubinin, R. Modolo, M. Fraenz, J. Woch, G. Chanteur, F. Duru, F. Akalin, D. Gurnett, R. Lundin, S. Barabash, J. Winningham, R. Frahm, J. Plaut and P. G, *Journal of Geophysical Research, v.113 (2008)*, 2008, **113**,.

[9] L. Frank, W. Paterson and K. Khurana, *J. Geophys. Res.*, 2002, **107**,.

[10] V. Dols and R. Johnson, *Icarus*, 2023, **392**, 115365.

[11] L. A. Frank, W. R. Paterson, K. L. Ackerson, V. M. Vasyliunas, F. V. Coroniti and S. J. Bolton, *Science*, 1996, **274**, 394–395.

[12] J. Lilensten, O. Witasse, C. Simon Wedlund, H. Dossmann, O. Dutuit, R. Thissen and C. Alcaraz, *Geophysical Research Letters - GEOPHYS RES LETT*, 2005, **32**,.

[13] J. Lilensten, C. Simon Wedlund, M. Barthélémy, R. Thissen, D. Ehrenreich, G. Gronoff and O. Witasse, *Icarus*, 2013, **222**, 169–187.

[14] M. C. McCarthy, K. L. K. Lee, R. A. Loomis, A. M. Burkhardt, C. N. Shingledecker, S. B. Charnley, M. A. Cordiner, E. Herbst, S. Kalenskii, E. R. Willis, C. Xue, A. J. Remijan and B. A. McGuire, *Nature Astronomy*, 2021, **5**, 176–180.

[15] K. L. K. Lee, B. A. McGuire and M. C. McCarthy, *Physical Chemistry Chemical Physics*, 2019, **21**, 2946–2956.

[16] B. A. McGuire, A. M. Burkhardt, S. Kalenskii, C. N. Shingledecker, A. J. Remijan, E. Herbst and M. C. McCarthy, *Science*, 2018, **359**, 202–205.

[17] S. Kalenskii, *arXiv: Astrophysics of Galaxies*, 2017.

[18] A. M. Burkhardt, R. A. Loomis, C. N. Shingledecker, K. L. K. Lee, A. J. Remijan, M. C. McCarthy and B. A. McGuire, *Nature Astronomy*, 2021, **5**, 181–187.

[19] J. Jose, A. Zamir and T. Stein, *Proceedings of the National Academy of Sciences*, 2021, **118**, e2101371118.

[20] J. Cernicharo, C. Cabezas, R. Fuentetaja, M. Agendez, B. Tercero, J. Janeiro, M. Juanes, R. I. Kaiser, Y. Endo, A. L. Steber, D. Perez, C. Perez, A. Lesarri, N. Marcelino and P. de Vicente, *Astronomy & Astrophysics*, 2024, **690**, L13.

[21] G. Wenzel, I. R. Cooke, P. B. Changala, E. A. Bergin, S. Zhang, A. M. Burkhardt, A. N. Byrne, S. B. Charnley, M. A. Cordiner, M. Duffy, Z. T. P. Fried, H. Gupta, M. S. Holdren, A. Lipnicky, R. A. Loomis, H. T. Shay, C. N. Shingledecker, M. A. Siebert, D. A. Stewart, R. H. J. Willis, C. Xue, A. J. Remijan, A. E. Wendlandt, M. C. McCarthy and B. A. McGuire, *Science*, 2024, **0**, eadq6391.

[22] D. Gupta, H. Choi, S. Singh, P. Modak, B. Antony, D.-C. Kwon, M.-Y. Song and J.-S. Yoon, *The Journal of Chemical Physics*, 2019, **150**, 064313.

[23] A. M. Rymer, A. J. Coates, K. Svenes, G. A. Abel, D. R. Linder, B. Narheim, M. Thomsen and D. T. Young, *Journal of Geophysical Research: Space Physics*, 2001, **106**, 30177–30198.

[24] A. M. Rymer, H. T. Smith, A. Wellbrock, A. J. Coates and D. T. Young, *Geophysical Research Letters*, 2009, **36**,.

[25] D. Snowden and R. Yelle, *Icarus*, 2014, **243**, 1–15.

[26] M. Galand, J. Lilensten, D. Toublanc and S. Maurice, *Icarus*, 1999, **140**, 92–105.

[27] H. Cottin, M. H. Moore and Y. Bénilan, *The Astrophysical Journal*, 2003, **590**, 874.

[28] T. Monfredini, H. M. Quitian-Lara, F. Fantuzzi, W. Wolff, E. Mendoza, A. F. Lago, D. A. Sales, M. G. Pastoriza and H. M. Boechat-Roberty, *Monthly Notices of the Royal Astronomical Society*, 2019, **488**, 451–469.

[29] H. M. Boechat-Roberty, R. Neves, S. Pilling, A. F. Lago and G. G. B. De Souza, *Monthly Notices of the Royal Astronomical Society*, 2009, **394**, 810–817.

[30] J. Loison, E. Hébrard, M. Dobrijevic, K. Hickson, F. Caralp, V. Hue, G. Gronoff, O. Venot and Y. Bénilan, *Icarus*, 2015, **247**, 218–247.

[31] V. A. Krasnopolsky, *Icarus*, 2014, **236**, 83–91.

[32] E. H. Wilson and S. K. Atreya, *Journal of Geophysical Research: Planets*, 2004, **109**,.

[33] G. H. Wannier, *Physical Review*, 1953, **90**, 817–825.

[34] M. Inokuti, *Reviews of Modern Physics*, 1971, **43**, 297–347.

[35] J. J. Sakurai and J. Napolitano, *Modern Quantum Mechanics*, Cambridge University Press, 2020.